STEM CELLS AND DEVELOPMENT
Volume 24, Number 21, 2015

DOI: 10.1089/scd.2015.0066

Dysregulation of Mitochondrial Functions and Osteogenic Differentiation in Cisd2-Deficient Murine Induced Pluripotent Stem Cells

Ping-Hsing Tsai,[1] Yueh Chien,[1,2,*] Jen-Hua Chuang,[2,3,*] Shih-Jie Chou,[1,*] Chian-Hsu Chien,[2,3] Ying-Hsiu Lai,[4] Hsin-Yang Li,[4–6] Yu-Lin Ko,[2,5] Yuh-Lih Chang,[1,7] Chen-Ying Wang,[5] Yung-Yang Liu,[2,3] Hsin-Chen Lee,[1,5] Chang-Hao Yang,[8] Ting-Fen Tsai,[9] Yi-Yen Lee,[3,10] and Shih-Hwa Chiou[1,2–4]

Wolfram syndrome 2 (WFS2) is a premature aging syndrome caused by an irreversible mitochondria-mediated disorder. Cisd2, which regulates mitochondrial electron transport, has been recently identified as the causative gene of WFS2. The mouse *Cisd2* knockout (KO) (*Cisd2*$^{-/-}$) recapitulates most of the clinical manifestations of WFS2, including growth retardation, osteopenia, and lordokyphosis. However, the precise mechanisms underlying osteopenia in WFS2 and *Cisd2* KO mice remain unknown. In this study, we collected embryonic fibroblasts from Cisd2-deficient embryos and reprogrammed them into induced pluripotent stem cells (iPSCs) via retroviral transduction with Oct4/Sox2/Klf4/c-Myc. Cisd2-deficient mouse iPSCs (miPSCs) exhibited structural abnormalities in their mitochondria and an impaired proliferative capability. The global gene expression profiles of *Cisd2*$^{+/+}$, *Cisd2*$^{+/-}$, and *Cisd2*$^{-/-}$ miPSCs revealed that Cisd2 functions as a regulator of both mitochondrial electron transport and Wnt/β-catenin signaling, which is critical for cell proliferation and osteogenic differentiation. Notably, *Cisd2*$^{-/-}$ miPSCs exhibited impaired Wnt/β-catenin signaling, with the downregulation of downstream genes, such as *Tcf1*, *Fosl1*, and *Jun* and the osteogenic regulator *Runx2*. Several differentiation markers for tridermal lineages were globally impaired in *Cisd2*$^{-/-}$ miPSCs. Alizarin red S staining and flow cytometry analysis further revealed that *Cisd2*$^{-/-}$ miPSCs failed to undergo osteogenic differentiation. Taken together, our results, as determined using an miPSC-based platform, have demonstrated that Cisd2 regulates mitochondrial function, proliferation, intracellular Ca^{2+} homeostasis, and Wnt pathway signaling. Cisd2 deficiency impairs the activation of Wnt/β-catenin signaling and thereby contributes to the pathogeneses of osteopenia and lordokyphosis in WFS2 patients.

Introduction

Iron-sulfur cluster-containing proteins play pivotal roles in electron transfer in several biochemical processes, such as oxidative-reduction reactions and enzymatic activities [1]. CDGSH iron-sulfur domain-containing proteins include three major members, Cisd1, Cisd2, and Cisd3. These proteins contain a transmembrane helix, a CDGSH domain, and an iron-binding motif [2]. The Cisd family is thought to play a role in regulating oxidation. Cisd1 and Cisd3 are involved in regulation of electron transport and oxidative phosphorylation [3]. In addition to its role as an electron transport mediator, recent studies have indicated that Cisd2 may be involved in Ca^{2+} homeostasis [4,5]. Cisd1 and Cisd2 primarily function in mediating mitochondrial physiology [2].

However, the functions of the novel protein Cisd3, which contains two CDGSH domains and no transmembrane domain, remain unclear. Patients with a Cisd2 homozygous mutation are diagnosed with Wolfram syndrome 2 (WFS2), an autosomal recessive inherited disease characterized by juvenile-onset neurodegeneration of the central and peripheral nervous systems [6]. Chen et al. generated *Cisd2* knockout (KO) mice that exhibited WFS2-like clinical symptoms, including early senescence, protruding ears, corneal opacities,

[1]Institute of Pharmacology, [3]Institute of Clinical Medicine, [4]Institute of Anatomy & Cell Biology, [5]School of Medicine, [9]Department of Life Sciences & Institute of Genome Sciences, National Yang-Ming University, Taipei, Taiwan.
[2]Department of Medical Research, Taipei Veterans General Hospital, Taipei, Taiwan.
Departments of [6]Obstetrics and Gynecology, [7]Pharmacy, and [10]Neurosurgery, Neurological Institute, Taipei Veterans General Hospital, Taipei, Taiwan.
[8]Department of Ophthalmology, National Taiwan University Hospital, Taipei, Taiwan.
*These authors contributed equally to this work.

thin bones, and low muscle mass [7]. Mitochondrial biogenesis and dynamic homeostasis are important for supplying a sufficient amount of energy for development and differentiation [8]. Notably, Chen et al. have demonstrated that Cisd2 deficiency leads to structural damage of the outer mitochondrial membrane in mice, resulting in mitochondrial dysfunction with reduced electron transport activity and oxygen consumption. However, whether Cisd2 affects mitochondrial function to further modulate stem cell biology and cellular differentiation during early development remains unclear.

Mitochondria depend on the activity of the mitochondrial electron transport chain, as mediated by respiratory complexes I, III, and IV, which drive ATP synthesis through complex V (ATP synthase) [9]. Mitochondrial electron transport generates not only ATP but also by-products, including ROS and other metabolites [10]. In mitochondrial oxidative phosphorylation, mitochondria generate more ATP and ROS than is produced by glycolysis. Mitochondria are necessary for supporting active proliferation; therefore, they are essential for cell reprogramming and maintaining human embryonic stem cell identity [11]. Mitochondria regulate cell proliferation and differentiation, particularly in osteoblasts and adipocytes [12–14]. Consistent with these functions, the inhibition of mitochondrial respiration via chemical treatments or overexpression of transcription factors increases pluripotency, whereas activation of mitochondrial activity impairs reprogramming [10].

The intracellular distribution of mitochondria has been associated with the degree of stemness in adult monkey stromal stem cells [15], suggesting that their differential distribution affects the maturation of developing embryonic stem cells [16]. Gene KOs of critical factors (*Tfam*, *Polg*, and *Polg2*) in mitochondrial biogenesis cause embryonic lethality at a late stage due to an insufficient supply of energy and metabolites required for cell differentiation [17]. Mitochondrial inhibitors retard osteogenic differentiation [18]. Similarly, Cisd2 modulates the differentiation of adipocytes by regulating intracellular Ca^{2+} homeostasis [19]. However, how the loss of Cisd2 delays differentiation remains unclear. A recently developed promising technique for recapitulating developmental and pathological processes involves the reprogramming of differentiated human/mouse somatic cells into induced pluripotent stem cells (iPSCs) [20,21].

iPSCs are generated by transducing 4 transcription factor-encoding genes, known as the OSKM genes, including Oct4 (Pou5F1), Sox2, Klf4 (Kruppel-like factor 4), and c-Myc, and these cells have been confirmed to exhibit embryonic stem cell-like characteristics in studies of the mechanisms and progression of diseases and in medical applications [21]. In this study, we established *Cisd2* KO mouse iPSCs (miPSCs), representing naïve precursors to multiple lineages present in Wolfram syndrome. We sought to elucidate the transcript profile of these Cisd2-deficient miPSCs and mitochondria-associated parameters to further evaluate the specific role of Cisd2 in transcriptional regulation. The capacity of Cisd2-deficient miPSCs for differentiation into multiple lineages, particularly osteogenic lineages, was also investigated. The results of this study allow elucidation of the role of Cisd2 in mitochondria and suggest that this protein maintains the expression of developmental genes by affecting Wnt signaling.

Materials and Methods

Generation of iPSC lines and cell culture

Cisd2 deficiency ($Cisd2^{+/-}$, $Cisd2^{-/-}$) and wild-type ($Cisd2^{+/+}$) C57BL/6 mice have been described [7]. The mice were bred and treated according to the National Research Council's Guide for the Care and Use of Laboratory Animals. Fibroblasts were collected from postnatal mice, and cultured in DMEM medium supplemented 15% fetal bovine serum (FBS). For reprogramming into iPSCs, fibroblasts were plated at 1×10^5 cells per six-well dish for infection with OSKM retrovirus. After infection, cells were cultured and medium changed every 2 days. After 16 days, embryonic stem cells like colonies were transferred onto feeder layer and cultured in DMEM supplemented with 15% FBS, 0.1 mM nonessential amino acids (11140-050; Invitrogen), 0.55 mM 2-mercaptoethanol (M7154-100 ML; Sigma), 50 μg/mL penicillin-streptomycin (15140-122; Invitrogen), and 0.3% recombinant leukemia inhibitory factor (LIF, PMC9484; Invitrogen) at 37°C, 5% CO_2. $Cisd2^{+/+}$, $Cisd2^{+/-}$, and $Cisd2^{-/-}$ miPSCs were cultured in the ES medium supplemented with LIF.

Embryoid body-mediated osteogenic differentiation

For embryoid body (EB) formation, miPSCs were dissociated into a single cell suspension using 0.25% trypsin-EDTA and plated onto nonadherent bacterial culture dishes at a density of 2×10^6 cells/100 mm plate, where they were allowed to aggregate. After 4 days in floating culture, EBs were transferred onto gelatin-coated plates and maintained in the same medium for 24 h. EBs were then assigned to different groups for in vitro differentiation into multiple lineages as previously described [22], including hepatic, adipogenic, and neural differentiation lineages. Next, EBs were transferred to gelatin-coated plates and cultured with osteogenic induction medium (DMEM-HG containing 10% FBS, 10^{-8} M dexamethasone, 50 μg/mL ascorbic acid, 10 mM β-glycerolphosphate, and 1% penicillin-streptomycin). For osteogenic differentiation, cells were cultured at 37°C and 5% CO_2 for 21 days, and the medium was changed every other day.

Teratomas assay

miPSCs were maintained and propagated on the feeder cell. Three days later, miPSCs were trypsinized, washed twice with phosphate buffered saline (PBS), and then subcutaneously injected into the bilateral inguens of male NOD-SCID mice (3×10^7 cells per mL in saline, 100 μL per injection). After 3–4 weeks, teratoma were collected and fixed in 4% paraformaldehyde, before embedding in paraffin. This study was approved by the Institutional Review Board (VGHIRB 2014-05-002C) of Taipei Veterans General Hospital. Paraffin-embedded tissue was sectioned and stained with H&E.

Chimera mouse production by blastocyst injection

The introduction of $Cisd2^{+/+}$ and $Cisd2^{-/-}$ miPSCs (derived from C57BL/6J strain, black coat color) into mouse blastocysts-derived from C57BL/6J-Tyrc2J strain (albino) was followed as previously described with some modifications [23]. The adult chimeras were confirmed by coat color,

demonstrating that miPSCs were competent to produce adult chimeric mice. This study was assisted by the Transgenic Mouse Model Core Facility, Academic Sinica, Taiwan.

Alkaline phosphatase staining

For detecting the alkaline phosphatase (AP) activity of cells on original plates, cells were fixed with 80% alcohol, and then fixed cells stained using the Blue Alkaline Phosphatase Substrate kit III (Vector Laboratories) according to the manufacturer's instructions.

Western blot analysis, immunofluorescence assay, and flow cytometry

Western blots were performed as previously described [22]. Details of antibodies can be found in Supplementary Table S1 (Supplementary Data are available online at www.liebertpub.com/scd). Antigen–antibody complexes were visualized by using an enhanced chemiluminescence detection kit (GE Healthcare Bio-Sciences Corp.). For data quantification, films were scanned with a CanonScan 9950F scanner; the acquired images were then analyzed on a Macintosh computer using the public domain NIH ImageJ program (at http://rsb.info.nih.gov/nih-image/).

Cells were fixed with 4% paraformaldehyde, permeabilized in 1% triton X-100, and blocked with 5% FBS. Cells were stained with primary antibodies, and then incubated with Alexa Fluor 568-conjugated anti rabbit (1:300; Invitrogen) or FITC-conjugated anti rabbit (1:300; Invitrogen). Details of antibodies can be found in Supplementary Table S1. Cells were then washed with PBS and photographed under a fluorescence microscope (Olympus).

Membrane potential ($\Delta\psi m$) and mitochondrial mass

$\Delta\psi m$ was assessed in the iPSC lines using a MitoProbe JC-1 Assay Kit by flow cytometry (Life Technologies), according to the manufacturer's protocol. Briefly, miPSCs were seeded on six-well plates at a density of 5×10^5 cells/well and cultured for 1 day. The cells were then resuspended in 500 μL of warm media and incubated with JC-1 dye (2 mM final concentration) at 37°C and 5% CO_2 for 30 min and washed twice with PBS before flow cytometry analysis. At high concentrations, JC-1 monomers form aggregates. The monomers emit green fluorescence, and the aggregates emit red fluorescence. A decrease in delta psi is determined according to a decrease in red fluorescence emission [24,25], and a decrease in monomeric fluorescence (JC-I green) indicates a loss of mitochondrial mass [26]. Cells were collected via centrifugation and resuspended in PBS. The relative membrane potential was calculated by normalizing the intensity of red JC-1 fluorescence to that of green JC-1 fluorescence, which represents the mitochondrial mass. The samples were analyzed by flow cytometry (BD LSRFortessa cell analyzer; Becton Dickenson) and BD FACS Diva software (Becton Dickenson).

To determine mitochondrial mass, miPSCs were seeded on six-well plates at a density of 5×10^5 cells/well and cultured for 1 day. The cells were then trypsinized, suspended in PBS, and transferred into flow tubes. One millimolar 10-N-nonyl acridine orange (NAO) dye was added to the tubes, which were protected from light, for 10 min at room temperature. The fluorescence intensity of 10,000 cells, as determined by flow cytometry, was recorded at an excitation wavelength of 488 nm and an emission wavelength of 535 nm.

Quantitative real-time polymerase chain reaction

Total mRNA was obtained using RNeasy kit (Qiagen) reverse-transcribed using the superscript III first strand synthesis system (Invitrogen). Quantitative polymerase chain reaction was carried out with ABI 7900 Fast System and SYBR Green Master Mix. Primer sequences are shown in Supplementary Tables S2 and S3. The expression values are normalized against the corresponding Gapdh value.

Transmission electron microscopy

miPSCs were fixed in the mixture of glutaraldehyde and paraformadehyde in cacodylate buffer (pH 7.4). They were postfixed in 1% OsO_4 and 1.5% potassium hexanoferrate (pH 6.0), then rinsed in cacodylate and 0.2 M sodium meleate buffers (pH 6.0), and blocked with 1% uranyl acetate. Following dehydration, the cells were embedded in Epon and sectioned for TEM analysis.

Cell growth rate and MTT assay

For evaluation of cell growth rate, miPSCs were plated on 24-well plates at a density of 2×10^4 cells/well. Cells were trypsinized and determined by cell counting at day 0, 1, and 3. For determination of viable cell number at different passage, cells were seeded on 24-well plates at a density of 2×10^4 cells/well. After aspirating the culture medium, cells were incubated with DMEM medium with the addition of methyl thiazol tetrazolium (3-(4,5-dimethylthiazoyl-2)-2,5-dipheyl tetrazolium bromide at 0.5 mg/mL; SIMGA) at 37°C for 1 h. After incubation, we aspirated the medium and added dimethyl sulfoxide to dissolve the MTT formazan product. The amount of MTT formazan product was determined using a microplate reader at an absorbance of 560 nm (SpectraMax 250; Molecular Devices).

Microarray, gene set enrichment analysis, and ingenuity pathway analysis

Total RNA was extracted from mouse *Cisd2*$^{+/+}$, *Cisd2*$^{+/-}$, and *Cisd2*$^{-/-}$ miPSCs using an RNeasy Kit (Qiagen). Reverse transcription and hybridization were performed at the gene expression analysis core facility of the National Yang-Ming University Genome Research Center. Arrays (Affymetrix Mouse 430A 2.0) processed according to the manufacturer's instructions were scanned using an Affymetrix microarray platform. Raw microarray data were preprocessed and normalized using the RMA algorithm implemented in Affymetrix Power Tools. The expression levels of individual genes were calculated by averaging the signal intensities of all of the corresponding probesets. Heatmap and hierarchical clustering was performed for selected RNAs based on city-block distances. The distances were computed based on the average mRNA expression levels in the mouse *Cisd2*$^{+/+}$, *Cisd2*$^{+/-}$, *Cisd2*$^{-/-}$ miPSC, and mESC groups. The genes used for functional classification in Fig. 2B are listed in Supplementary Table S4. To gain

functional insights from these gene expression data, gene set enrichment analysis (GSEA) was conducted using predefined gene sets (ectoderm, mesoderm, and endoderm) [27–29] and a customized R script for GSEA. The datasets were submitted to Gene Expression Omnibus database (www.ncbi.nlm.nih.gov/geo). The differentially expressed genes between the *Cisd2*$^{+/+}$ and *Cisd2*$^{-/-}$ miPSCs were imported into ingenuity pathway analysis (IPA) software (Ingenuity® Systems, http://www.ingenuity.com) for functional and pathway analyses.

Alizarin red S staining

Following previous described osteogenic differentiation method, the ability of calcium deposition was determined at day 21. After aspirating the culture medium, cells were washed with PBS. Ice-cold 70% alcohol was added to fix the cells. After fixing for 1 h, cells were washed thrice with ddH_2O. Twenty millimolars alizarin red S (ARS) solution was added into each well and incubated for 20 min. After aspirating the solution, cells were washed thrice with ddH_2O. After aspirating the solution, CPC buffer [10 g cetylpyridinium chloride (CPC; Sigma) and 0.1469 g Na_2HPO_4 (Sigma) dissolved in 100 mL ddH_2O] was added and then incubated for 1 h. The amount of ARS was determined at an absorbance of 405 nm (SpectraMax 250; Molecular Devices).

Flow cytometry analysis for HCC cell lines

To detect the expression profiles of alkaline phosphatase (ALP) in each miPSC lines, cells were incubated with rabbit anti-ALP antibody (AF2910; R&D Systems) and visualized by using Alexa 568-conjugated goat anti-mouse (Invitrogen). Samples were analyzed using an LSR II flow cytometry and CellQuest Software (BD Biosciences). Live cells were gated, and dead cells and cell debris were excluded using FCS and SSC biparametric plots.

Free intracellular Ca^{2+} measurement

Intracellular Ca^{2+} levels were determined using a Fluo3-AM probe (Molecular Probes), which binds Ca^{2+} with high specific affinity. After trypsinization, cells were washed once with Ca^{2+}-free PBS and resuspended in fresh buffer. The cells were then incubated in the dark with 5 μM Fluo-3/AM at 37°C for 30 min, and fluorescence was measured at FL-1 (530 nm) by flow cytometry (BD LSRFortessa cell analyzer; Becton Dickinson), with excitation at 488 nm. The fluorescence intensities of the Fluo-3/AM probes were measured via flow cytometry and analyzed using BD FACS Diva software (Becton Dickenson). At least 10,000 events per sample were acquired. Samples without Fluo-3AM fluorescence were considered blank controls, for which fluorescence was represented as F0. The Geo Mean of fluorescence (F) of each sample was subtracted by F0 to eliminate background fluorescence.

Immunoprecipitation assay

miPSCs were lysed in Buffer G, incubated overnight with 6 μg antibody, and captured with Protein G beads according to manufacturer's instructions. Two milligrams cell lysate was incubated with 20 μg Protein G beads. Protein complexes were eluted by boiling in loading buffer. Ten microliters was used for each immunoblot with 2% input.

Statistical analysis

Data were expressed as mean ± SD. Statistically significant differences among groups were detected by one-way analysis of variance, and when significance was observed, post hoc Tukey tests were performed using SPSS (SPSS 12.0; SPSS). Data were plotted using GraphPad Prism program (GraphPad Prism 5.0; GraphPad). The criterion for significance was set as $P < 0.05$.

Results

Characterization of Cisd2-deficient miPSCs

The somatic fibroblasts used to generate iPSCs were collected from Cisd2-deficient embryos, which carried mitochondria-associated phenotypic defects. However, whether cells containing the mutation for the genetic disease that causes premature aging can be reprogrammed into miPSCs is unknown. Cisd2 is an important regulator of life span [30]. *Cisd2* KO mice exhibit features of severe premature aging and early onset degeneration of multiple tissues. Most of these degenerated tissues were originally considered as mitochondria-enriched or dependent tissues. Thus, we attempted to determine whether Cisd2 deficiency affects miPSC generation. Cisd2 deficiency causes mitochondria-associated phenotypic defects in mice [7]. *Cisd2* KO mice have been demonstrated with many manifestations of premature aging, such as osteopenia, lordokyphosis, early onset degeneration of central nerves, and impaired glucose tolerance [7]. Systemic defects have been attributed to the differential global distribution and dysregulation of mitochondria. However, little is known about the potential role of the Cisd2-mediated developmental process in developing blastocysts. Indeed, Cisd2 deficiency has been reported to delay adipocyte differentiation. Considering the relative difficulty in obtaining sufficient embryos from *Cisd2*$^{-/-}$ mice and in culturing embryos in vitro for long periods of time, we established an iPSC-based model to develop an efficient platform for investigating Cisd2. To establish this model, we reprogrammed Cisd2-deficient fibroblasts using the OSKM genes. We collected individual fibroblasts from aging C57BL/6 (B6) mice with the *Cisd2*$^{+/+}$, *Cisd2*$^{+/-}$, and *Cisd2*$^{-/-}$ genotypes and then plated 4×10^4 cells/well in six-well plates 1 day before viral infection. We subsequently transduced fibroblasts with the OSKM genes on day 0. We observed an ES-like morphology in the reprogrammed fibroblasts by day 7 and detected ALP activity by day 18 (Fig. 1A). Finally, we obtained miPSCs with *Cisd2*$^{+/+}$, *Cisd2*$^{+/-}$, and *Cisd2*$^{-/-}$ genotypes via retroviral infection.

Before investigating whether the developmental process is affected by Cisd2 deficiency, we confirmed that Cisd2 expression in miPSCs was consistent with that in fibroblasts. Western blot analysis revealed that OSKM reprogramming had limited effects on the expression of this protein (Fig. 1B). We determined that Cisd2 expression was similar in *Cisd2*$^{+/+}$ mouse embryonic fibroblasts (MEFs) from primary culture from fetal mice, *Cisd2*$^{+/+}$ aging fibroblasts and miPSCs, suggesting that its expression was maintained at

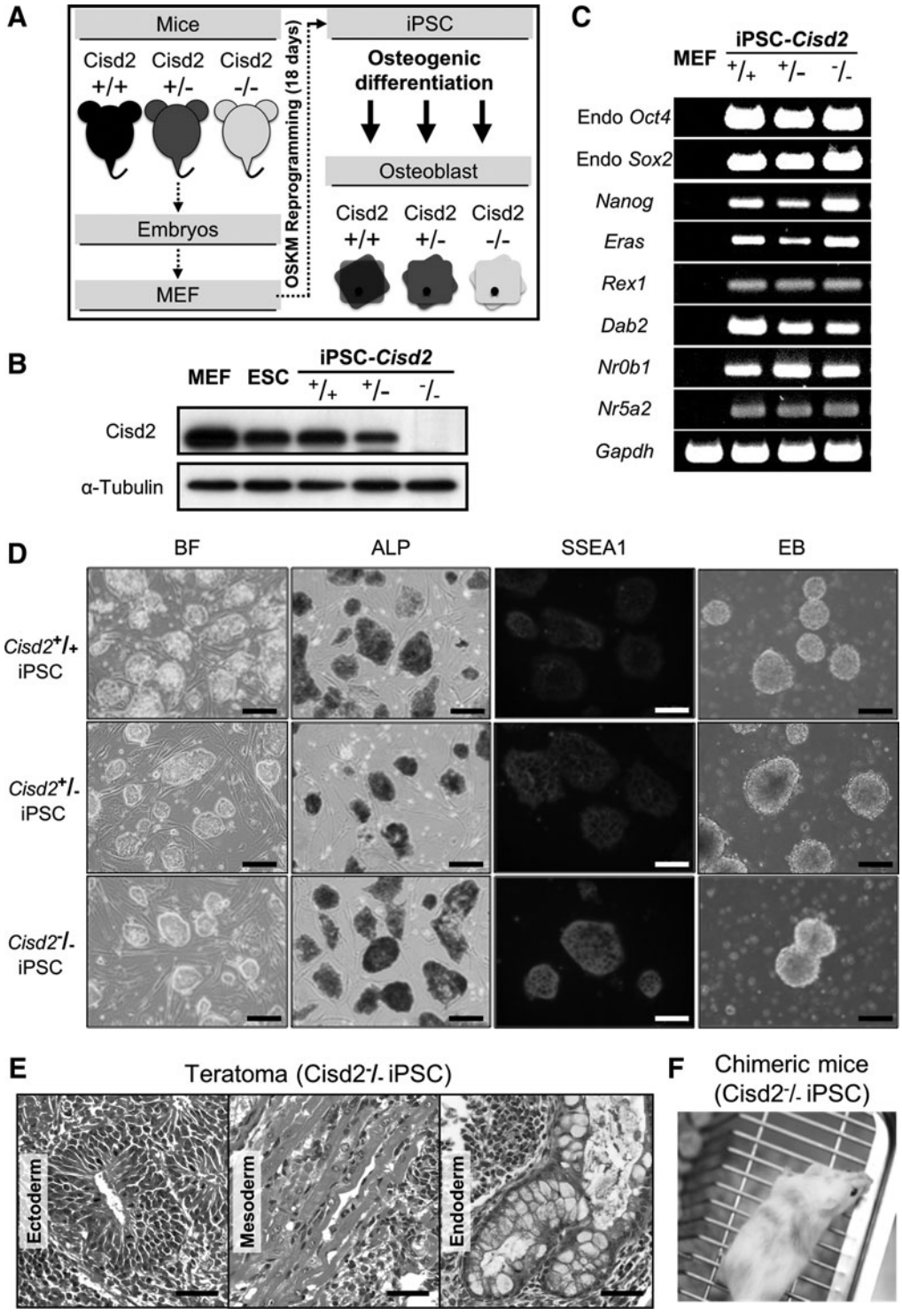

FIG. 1. Generation of miPSCs derived from wild-type ($Cisd2^{+/+}$) or Cisd2-deficient ($Cisd2^{+/-}$ and $Cisd2^{-/-}$) fibroblasts using the four OSKM factors. **(A)** Overview of the use of Cisd2-deficient miPSC lines for disease modeling. Mouse embryonic fibroblasts (MEF) from the $Cisd2^{+/+}$, $Cisd2^{+/-}$, and $Cisd2^{-/-}$ mice are reprogrammed through exogenous expression of transcription factors (Oct4, Sox2, Klf4, and c-Myc), tested for pluripotency then differentiated to relevant cell types in vitro. **(B)** Western blot analysis of Cisd2 expression in fibroblasts, embryonic stem cells, and the miPSC lines. α-Tubulin was used as a loading control. **(C)** RT-PCR analysis of stemness marker genes in the miPSC lines, including Endo-*Oct4*, Endo-*Sox2*, *Nanog*, *Eras*, *Rex1*, *Dab2*, *Dax1*, *Nr0b1*, and *Nr5a2*. *Gapdh* was used as a loading control. **(D)** Bright field (BF) image showing the morphology of undifferentiated miPSC lines grown on irradiated MEFs (Scale bar = 100 μm). Alkaline phosphatase (ALP) staining of the undifferentiated miPSC lines (Scale bar = 250 μm). Immunofluorescence staining analysis of SSEA1 in the miPSC lines (Scale bar = 100 μm). Embryoid body (EB) assay of the miPSC lines within 2–3 days. **(E)** miPSCs (3×10^6 cells) were subcutaneously inoculated into NOD-SCID mice. After 4 weeks, teratomas were sectioned and stained. Hematoxylin and eosin staining shows a teratoma from $Cisd2^{-/-}$ miPSCs containing multiple tissues, including neural epithelium (ectoderm), muscle (mesoderm), and glandular epithelium (endoderm) (Scale bar = 50 μm). **(F)** Chimeric mice (8 weeks old) produced by injection of $Cisd2^{-/-}$ miPSCs into eight-cell C57BL/6J-Tyrc2J embryos. iPSCs, induced pluripotent stem cells; miPSCs, mouse iPSCs; RT-PCR, reverse transcription–polymerase chain reaction.

similar levels in these different cells. In contrast, Cisd2 expression was significantly lower in *Cisd2*$^{+/-}$ and *Cisd2*$^{-/-}$ aging miPSCs than in *Cisd2*$^{+/+}$ miPSCs. These results indicated that retroviral infection of cells with the OSKM genes did not affect the expression of this Cisd2. Next, we examined the expression of pluripotency markers by reverse transcription–polymerase chain reaction (RT-PCR). RT-PCR analysis revealed that all of the stemness genes were expressed (Fig. 1C), including Endo-*Oct4*, Endo-*Sox2*, *Nanog*, *Eras*, *Rex1*, *Dab2*, *Nr0b1*, and *Nr5a2* [21]. Despite the absence of Cisd2, these iPSC colonies exhibited all of the characteristics of embryonic stem cells, including the characteristic morphology, ALP activity, expression of the stemness marker SSEA1 and formation of EBs (Fig. 1D). Collectively, our data demonstrated that the miPSCs with the genotypes *Cisd2*$^{+/+}$, *Cisd2*$^{+/-}$, and *Cisd2*$^{-/-}$ were embryonic stem cell-like. To further investigate the role of Cisd2 in regulating development in vivo, we transplanted Cisd2$^{-/-}$ miPSC cells (3×10^6 cells) subcutaneously into immune-compromised NOD-SCID mice. Teratoma-containing cells from the three germ layers, namely the ectoderm (neural epithelium, Fig. 1E), mesoderm (muscle, Fig. 1E), and endoderm (respiratory epithelium, Fig. 1E), were observed upon histological analysis, indicating that the cells had a considerable level of pluripotency. To further investigate the pluripotency of Cisd2-deficient cells, we performed a chimeric experiment to evaluate the developmental potential of Cisd2-deficient miPSCs. Notably, we obtained surviving *Cisd2*$^{-/-}$ chimeric mice by injecting Cisd2-deficient miPSCs into C57BL/6J-Tyrc2J blastocysts. Compared with the chimeric mice generated using *Cisd2*$^{+/+}$ miPSCs, live *Cisd2*$^{-/-}$ chimeric mice were distinguished based on their coat color (Fig. 1F), indicating that Cisd2-deficient miPSCs are still able to differentiate in vivo. These data indicate that the loss of Cisd2 does not inhibit iPSC generation and that miPSCs with this disease-causing mutation exhibit the typical capacity for simple differentiation in vitro.

Cisd2 regulates the membrane potential of iPSCs

Cisd2 is located in the ER and mitochondrial membrane and contains two redox-active 2Fe-2S clusters [7,31]. It may play a critical role in maintaining the integrity and function of mitochondria [7]. Interestingly, it is also a causative gene of a premature aging phenotype [7]. However, the consequences of Cisd2 deficiency in both somatic cells and stem cells are not yet fully understood. First, we evaluated the mitochondrial structure of Cisd2-deficient miPSCs. TEM analysis revealed normal mitochondrial structures in *Cisd2*$^{+/+}$ miPSCs but not in *Cisd2*$^{-/-}$ miPSCs (Fig. 2A). Only a few mitochondria were detected in *Cisd2*$^{-/-}$ miPSCs, in which cristae were rarely visible compared with those in *Cisd2*$^{+/+}$ miPSCs, suggesting an altered mitochondrial structure resulting from Cisd2 deficiency. A pie plot based on the microarray analysis results revealed six major classifications of predominantly downregulated transcripts in Cisd2$^{-/-}$ miPSCs, including mitochondrial localization, fission and fusion, inner membrane translocation, outer membrane translocation, mitochondrial protein import, and membrane polarization and potential (Fig. 2B). Among these classifications, Cisd2 predominantly affected the transcripts that function to maintain mitochondrial membrane polarization and potential.

Based on the findings of TEM and microarray analyses (Fig. 2A, B) and because Cisd2 has been demonstrated to be associated with mitochondrial dysfunction and degenerative disorders in aging mammals [7], we hypothesized that senescent somatic cells (MEFs) or senescent stem cells (iPSCs) would also exhibit notable abnormalities in mitochondrial function. Serial passages have been shown to induce cellular senescence [32]; therefore, we assessed and compared mitochondrial potentials ($\Delta\Psi$m) by JC-1 analysis [24] among cells with various Cisd2 genotypes (Cisd2$^{+/+}$, Cisd2$^{+/-}$, and Cisd2$^{-/-}$) at passages 1 to 5, and we investigated whether Cisd2 deficiency impairs the mitochondrial membrane potential in somatic cells or stem cells. In general, somatic cells (MEFs) with any given genotype exhibited a higher mitochondrial membrane potential. Remarkably, both MEFs and miPSCs showed signs of Cisd2 deficiency at higher passages (ie, they consistently exhibited impaired mitochondrial potentials; Fig. 2C). NAO assay also revealed decreased mitochondrial masses in Cisd2-deficient cells (MEFs and miPSCs) compared with their Cisd2$^{+/+}$ counterpart cells (Supplementary Fig. S1A). These results indicated that Cisd2 deficiency impaired regular mitochondrial functioning in both somatic and stem cells.

Several proteins have been closely associated with mitochondrial function. HS-1-associated protein X-1 (Hax-1), which is a mitochondrial protein with antiapoptotic functions, is a regulator of Ca^{2+} signaling. Hax-1 has been implicated in severe congenital neutropenia and neurological disorders [33]. BCL2/adenovirus E1B 19-kDa interacting protein 3 (*Bnip3*) encodes a mitochondrial outer membrane protein that is associated with cell death, membrane permeability, and the proton electrochemical gradient in normal tissues [34]. Superoxide dismutase 1 (*Sod1*) encodes a mitochondrial protein that converts harmful superoxide radicals into less toxic metabolites [35]. Tumor protein P53 (*Trp53*) encodes the most frequently mutated tumor suppressor in human cancers that is directly involved in mitochondrial outer membrane permeability [36]. To explore the mechanism associated with the mitochondrial dysfunction mediated by Cisd2 deficiency, we performed western blotting and quantitative real-time polymerase chain reaction (qRT-PCR) to examine the expression of mitochondria-associated factors in miPSC lines with various Cisd2 genotypes (Cisd2$^{+/+}$, Cisd2$^{+/-}$, and Cisd2$^{-/-}$). Western blot analysis revealed downregulation of the Hax1, Bnip3, and Sod1 proteins in Cisd2$^{-/-}$ cells but not in Cisd2$^{+/+}$ cells (Fig. 2D). qRT-PCR further revealed downregulation of several mitochondria-associated genes, including *Hax1*, *Brinp3*, *Sod1*, and *Trp53* (Fig. 2E). Taken together, our findings indicate that Cisd2 modulates regular mitochondrial function and the gene expression and integrity of several mitochondria-associated factors.

Cisd2 sustains activation of canonical Wnt signaling

Because a recent study has reported that Cisd2-deficient mice exhibit osteopenia and lordokyphosis at ~8 to 12 weeks of age [7], we investigated the extent to which the known transcriptional network regulates early development and the Wnt pathway. The formation of the mesoderm from embryonic stem cells depends on canonical Wnt/β-catenin signaling, and inhibition of endogenous Wnt signaling

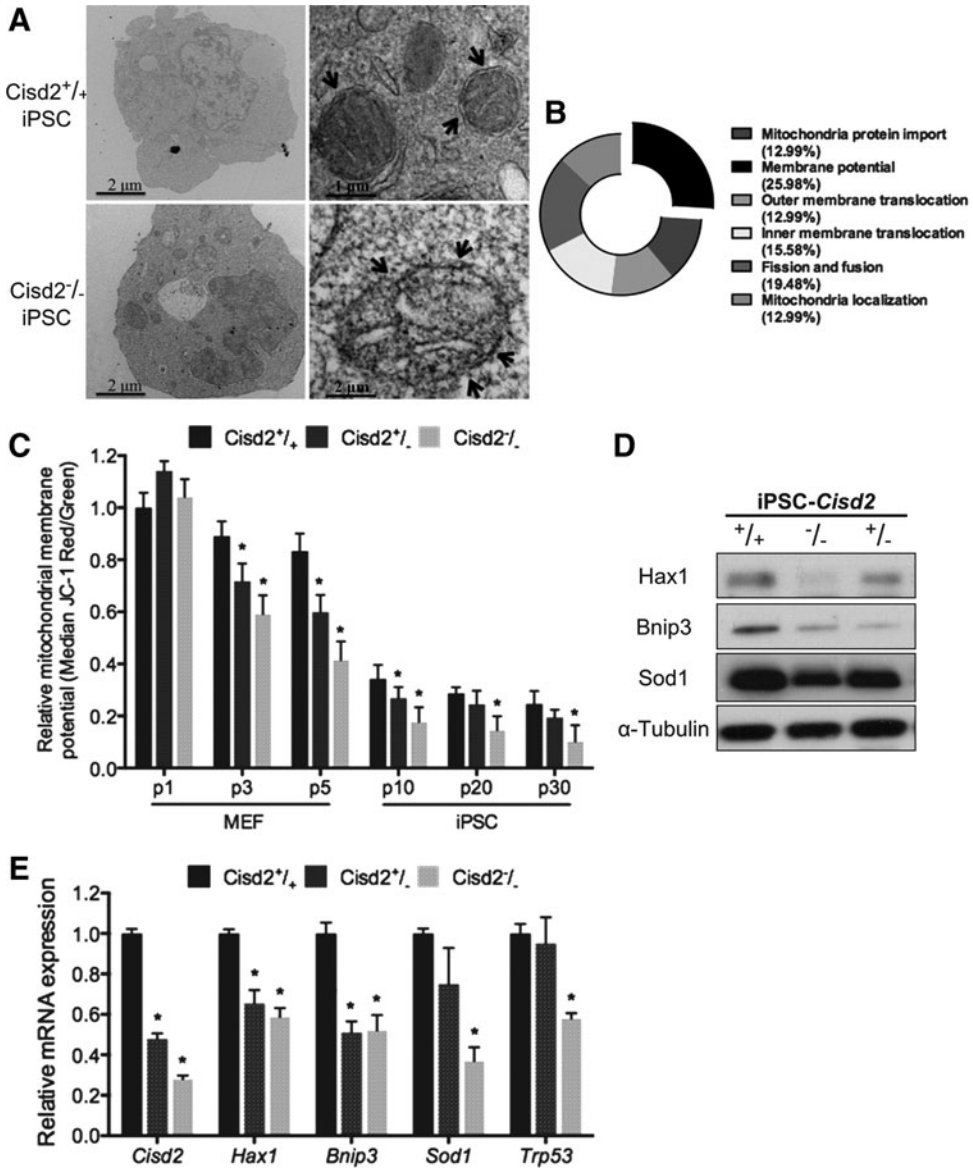

FIG. 2. Deficiency of Cisd2 in miPSCs results in the inhibition of the mitochondrial potential. **(A)** TEM analysis of the ultrastructure of the *Cisd2*$^{+/+}$ and *Cisd2*$^{-/-}$ miPSCs. *Arrows* indicate the mitochondria. **(B)** Pie plot showing the summary of mitochondria gene in *Cisd2*$^{-/-}$ miPSCs, including mitochondrial localization, fission and fusion, inner membrane translocation, outer membrane translocation, mitochondrial protein import, and membrane polarization and potential. Cisd2 deficiency impairs the ability to sustain the mitochondrial potential. **(C)** Mitochondria potential of different passage *Cisd2*$^{+/+}$, *Cisd2*$^{+/-}$, and *Cisd2*$^{-/-}$ fibroblasts (p1, p3, and p5) and miPSCs (p10, p20, and p30) were determined with JC-1 assay. **(D)** Western blots of mitochondria permeability protein in Cisd2$^{+/+}$, Cisd2$^{+/-}$, and Cisd2$^{-/-}$ miPSCs. Expression of Cisd2 protein maintains Hax1, Bnip3, and Sod1 expression. α-Tubulin was used as a loading control. **(E)** Quantitative RT-PCR analysis of the mitochondrial potential-associated genes in *Cisd2*$^{+/+}$, *Cisd2*$^{+/-}$, and *Cisd2*$^{-/-}$ miPSCs. Data represent mean ± SD in independent experiment. $^{*}P < 0.05$.

abolishes the differentiation potential toward the mesoderm and endoderm [37,38]. Early development genes exhibit Wnt-dependent expression, indicating that Wnt/β-catenin signaling plays an essential role in development. We performed microarray (Affymetrix mouse 430 2.0)-based analysis to compare the global transcript profiles of *Cisd2*$^{+/+}$, *Cisd2*$^{+/-}$, and *Cisd2*$^{-/-}$ miPSCs. We identified 2,267 (944 + 1,323) and 2,406 (1,083 + 1,323) genes that were downregulated in *Cisd2*$^{+/-}$ and *Cisd2*$^{-/-}$ miPSCs, respectively, compared with *Cisd2*$^{+/+}$ miPSCs. A comparison of the expression in these two groups revealed that 1,323 genes were significantly downregulated under Cisd2 deficiency (Fig. 3A). IPA (http://www.ingenuity.com/products/ipa) revealed the most relevant pathways associated with these overlapping genes (Fig. 3B). This analysis identified four relevant pathways, including the Wnt/β-catenin, human embryonic stem cell pluripotency, ERK/MAPK signaling, and estrogen receptor signaling pathways (all four pathways $P < 0.05$). In addition to being the most relevant among these pathways (Fig. 3B), Wnt signaling plays an important role in regulating the threshold and stability of responses to differentiation signals. Therefore, we specifically focused on the relationship between Cisd2 and the Wnt pathway. Hierarchical clustering analysis grouped all iPSCs with ESCs and not with MEFs (Fig. 3C). Clearly, the global expression pattern of *Cisd2*$^{-/-}$ miPSCs resembled that of ESCs, which are considered the gold standard of true pluripotency. Consistently, the expression of Wnt pathway members in *Cisd2*$^{-/-}$ miPSCs showed a less apparent correlation with that in ESCs (Fig. 3C), suggesting that Cisd2 may partially function to maintain the expression of transcripts. GSEA confirmed the results of IPA, demonstrating that putative Cisd2 genes were enriched in the Wnt pathway (Fig. 3D). Based on the IPA results, we identified the transcriptional regulatory network from our microarray results (Fig. 3E). Most of the downregulated genes in Cisd2-deficient miPSCs were closely linked with the Wnt pathway, suggesting that Cisd2 may regulate Wnt pathway signaling. To validate the regulatory effects of Cisd2 deficiency, we performed western blotting and qRT-PCR to evaluate the expression levels

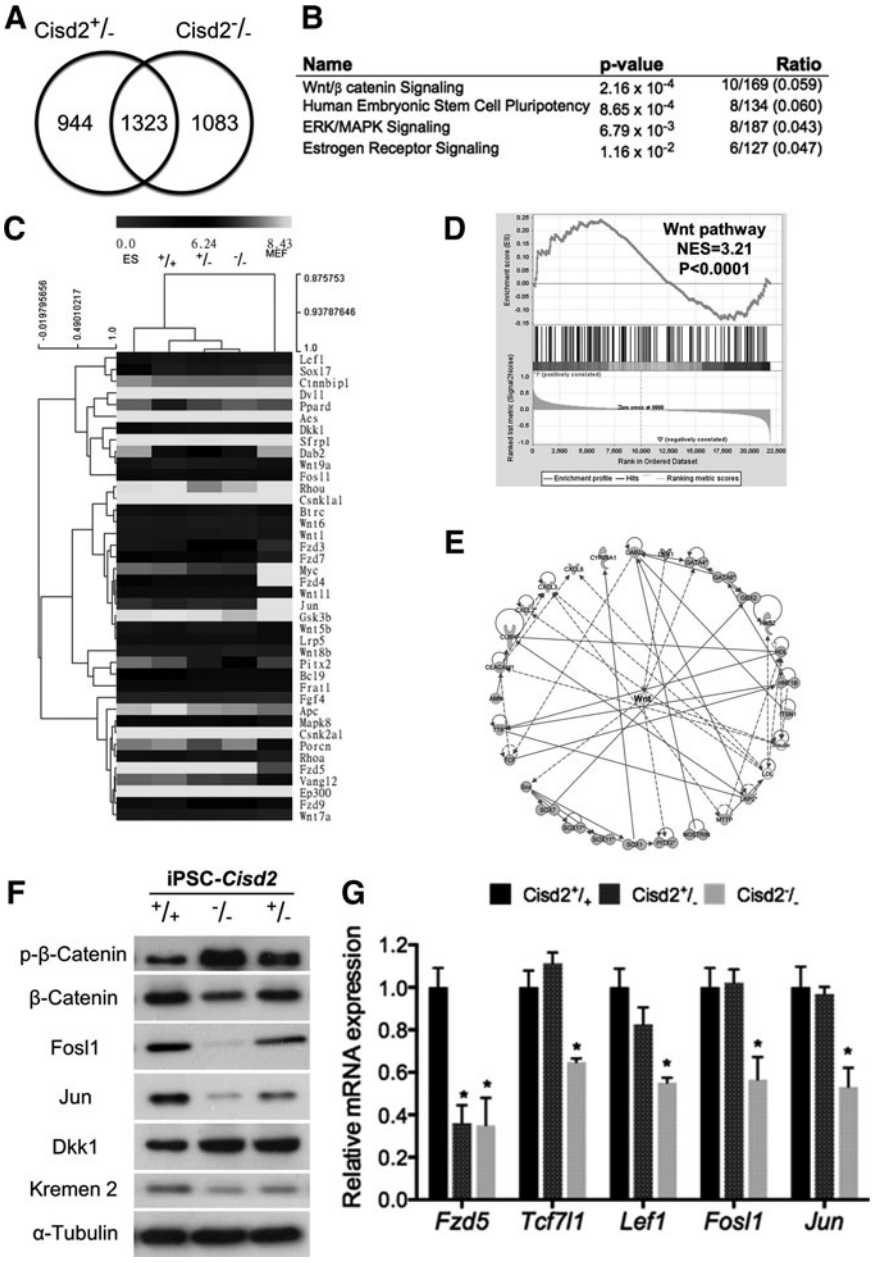

FIG. 3. Cisd2 deficiency impairs Wnt/β-catenin signaling. Microarray analysis is used to examine perturbation of endogenous gene expression by Cisd2 deficiency. **(A)** Overlapping downregulated genes in *Cisd2*$^{+/-}$ and *Cisd2*$^{-/-}$ miPSCs. **(B)** IPA analysis revealed the top four relevant pathways from the overlapping genes. **(C)** Heat map analysis and hierarchical clustering analysis revealed the similarity in the Wnt signaling-associated genes among the wild-type and Cisd2-deficient miPSCs. **(D)** GSEA analysis revealed a significant enrichment of Wnt-signaling. NES, normalized enrichment score. **(E)** Regulatory networks identified with IPA software for the overlapping genes that are downregulated in Cisd2$^{+/-}$ and Cisd2$^{-/-}$ iPSCs. The nodes in networks indicate a gene that is downregulated in Cisd2-deficient compared to the Cisd2-wild-type. *Solid lines* indicate a direct regulation, whereas *dashed lines* indicate a indirect regulation. **(F)** Western blot analysis of the Wnt-associated proteins in the *Cisd2*$^{+/-}$ and *Cisd2*$^{-/-}$ miPSCs. α-Tubulin was used as a loading control. **(G)** The expression levels of the Wnt downstream genes were analyzed in the *Cisd2*$^{+/+}$, *Cisd2*$^{+/-}$, and *Cisd2*$^{-/-}$ miPSCs. Data represent mean ± SD in independent experiment. $*P < 0.05$. GSEA, gene set enrichment analysis; IPA, ingenuity pathway analysis.

of several targets and/or regulators of the Wnt pathway. The Wnt/β-catenin pathway is a Wnt pathway that causes accumulation of β-catenin in the cytoplasm and its eventual translocation to the nucleus to act as a coactivator of transcription factors that belong to the Tcf/Lef family. Phosphorylation of β-catenin prevents its translocation into the nucleus and subsequently promotes its proteasome-mediated degradation [39]. In addition, *Fzd5*, *Tcf7l1*, and *Lef1* encode terminal effectors in Wnt signaling, and this signaling pathway induces *Fosl1* and *Jun* expression. *Fosl1* encodes a protein that dimerizes with Jun family proteins to form a transcription factor complex, AP-1. The AP-1 cell signaling pathway leads to cell apoptosis, survival, and proliferation [40]. We found that β-catenin phosphorylation was elevated in Cisd2$^{-/-}$ miPSCs compared with Cisd2$^{+/+}$ miPSCs, whereas the amount of total β-catenin was moderately decreased (Fig. 3F). In addition, Cisd2 deficiency resulted in a significant reduction in Fosl1 and Jun expression in Cisd2$^{-/-}$ miPSCs (Fig. 3F). Both Dkk1 and Kremen2 have been reported to be regulators of Wnt signaling [41]; therefore, we evaluated whether Cisd2 deficiency also affects these regulators and found that it had no effect on Kremen2 expression but that it led to the substantial upregulation of Dkk1 (Fig. 3F), indicating that Cisd2 may indirectly regulate the Wnt pathway via modulation of Dkk1 expression. qRT-PCR further revealed the downregulation of *Fzd5*, *Tcf7l1*, *Lef1*, *Fosl1*, and *Jun* in *Cisd2*$^{-/-}$ miPSCs compared with *Cisd2*$^{+/+}$ miPSCs (Fig. 3G). Taken together, these findings demonstrate that Cisd2 closely regulates the Wnt pathway and that this regulation may be partially modulated by Dkk1.

Cisd2 deficiency impairs the proliferative ability of miPSCs

To investigate the role of Cisd2 in the Wnt pathway, we investigated whether proliferation was affected by Cisd2 deficiency. Although mitochondria are important for cell proliferation, pluripotent stem cells rarely rely on mitochondria-mediated oxidative phosphorylation [8]. We performed GSEA, and the results further confirmed that most of the genes regulated by Cisd2 were closely associated with cell proliferation (Fig. 4A). To further quantitatively investigate the genes that participate in regulating cell proliferation, we performed qRT-PCR to determine the expression of the genes that were examined in GSEA. *Apc*, *EP300*, *Dab2*, and *c-Myc* are important transcriptional regulators that promote cell proliferation [42]. In addition, PCNA and MKi67 are highly expressed in the cells with high proliferation rates [42]. The expression levels of *Apc*, *EP300*, *Dab2*, *c-Myc*, *PCNA*, and *Ki67* were downregulated in $Cisd2^{-/-}$ miPSCs compared with $Cisd2^{+/+}$ miPSCs (Fig. 4B). Western blot analysis also indicated that Cisd2 deficiency decreased the EP300, Dab2, and PCNA levels, whereas the Apc level was unchanged (Fig. 4C).

To investigate whether Cisd2 regulates cell proliferation, we evaluated and compared the proliferation rates of MEFs and miPSCs with various *Cisd2* genotypes ($Cisd2^{+/+}$, $Cisd2^{+/-}$, or $Cisd2^{-/-}$) within 72 h. In MEFs at higher passages (fifth passage), the doubling time of $Cisd2^{-/-}$ MEFs was significantly higher than that of $Cisd2^{+/+}$ MEFs (Fig. 4D). At the 10th

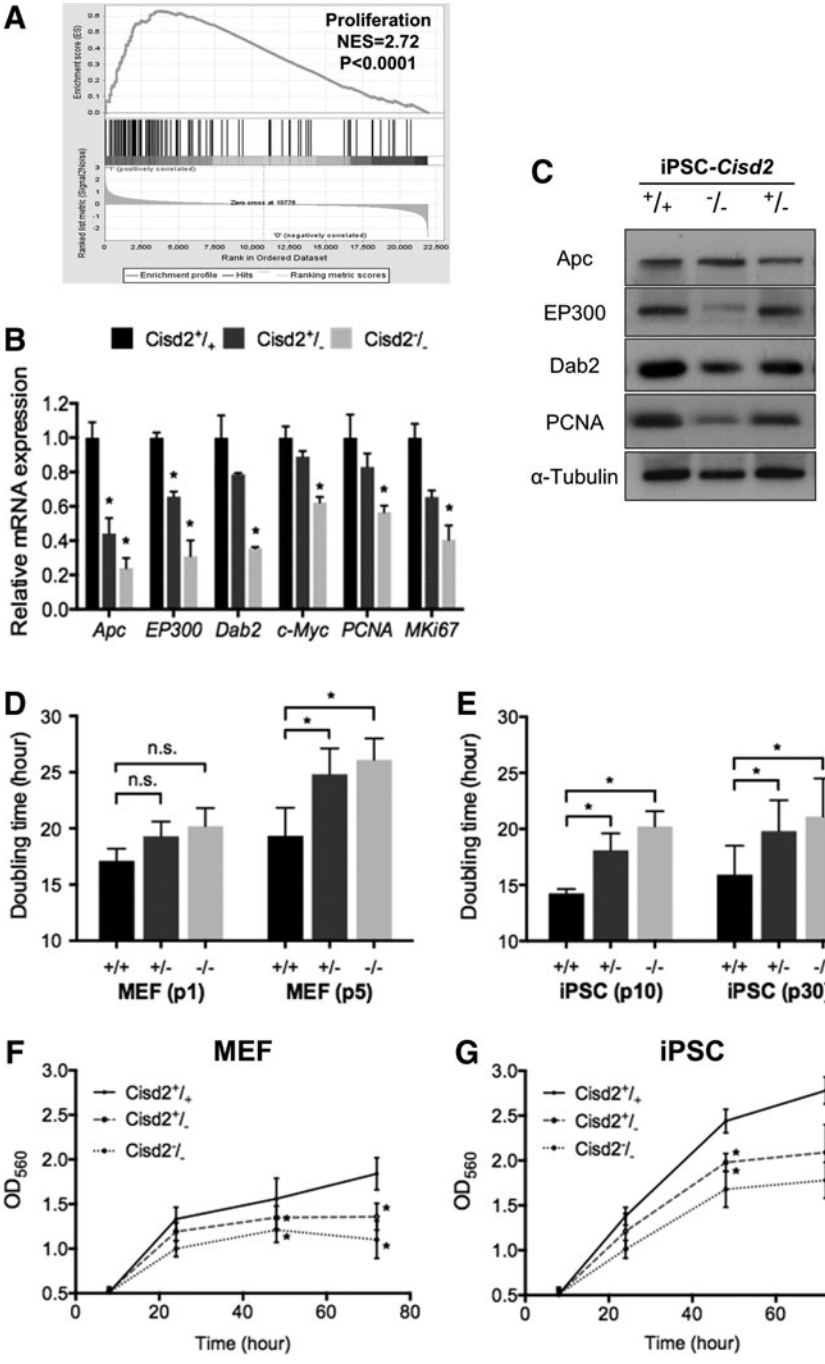

FIG. 4. Cisd2 deficiency impairs cell proliferation. **(A)** GSEA analysis revealed a significant enrichment in proliferation. NES, normalized enrichment score. **(B)** The expression levels of the proliferation-associated genes were analyzed in $Cisd2^{+/+}$, $Cisd2^{+/-}$, and $Cisd2^{-/-}$ miPSCs. **(C)** Western blot analysis of the proliferation-associated proteins in the $Cisd2^{+/+}$, $Cisd2^{+/-}$, and $Cisd2^{-/-}$ miPSCs. α-Tubulin was used as a loading control. **(D)** Comparison of cell doubling time measured in early (first passage) and late passage (fifth passage) $Cisd2^{+/+}$, $Cisd2^{+/-}$, and $Cisd2^{-/-}$ fibroblasts. **(E)** Comparison of cell doubling time measured in early (10th passage) and late passage (30th passage) $Cisd2^{+/+}$, $Cisd2^{+/-}$, and $Cisd2^{-/-}$ miPSCs. **(F)** MTT proliferation assays of $Cisd2^{+/+}$, $Cisd2^{+/-}$, and $Cisd2^{-/-}$ fibroblasts. **(G)** MTT proliferation assays of $Cisd2^{+/+}$, $Cisd2^{+/-}$, and $Cisd2^{-/-}$ miPSCs. Data represent mean ± SD in independent experiment. $^{*}P < 0.05$.

passage of miPSCs, *Cisd2*$^{-/-}$ miPSCs also exhibited a longer doubling time than their counterpart *Cisd2*$^{+/+}$ miPSCs, and the doubling time of miPSCs slightly increased at the 30th passage for all Cisd2 genotypes (Fig. 4E). MTT assay further revealed that the proliferative capacities of Cisd2-deficient MEFs (5th passage) and Cisd2-deficient miPSCs (30th passage) were significantly decreased compared with those of their Cisd2$^{+/+}$ counterpart cells (Fig. 4F, G, respectively). Collectively, our data demonstrate that Cisd2-deficient MEFs and miPSCs exhibit reduced proliferation rates, demonstrating a crucial role of Cisd2 in maintaining cell proliferation in both somatic and pluripotent stem cells.

Cisd2 deficiency impairs osteocyte differentiation

Because the Wnt pathway is essential for the development of embryonic stem cells, we hypothesized that Cisd2 deficiency may impair the development and differentiation of stem cells into various dermal lineages. To evaluate whether the differentiation capacity of Cisd2-deficient miPSCs was impaired, we assessed three germ layer markers after employing various differentiation protocols in miPSCs with various Cisd2 genotypes (*Cisd2*$^{+/+}$, *Cisd2*$^{+/-}$, or *Cisd2*$^{-/-}$). Immunofluorescence staining showed that miPSCs with each Cisd2 genotype were capable of tri-dermal differentiation in vitro and expressed the typical markers corresponding to each lineage, including alpha-fetoprotein, smooth muscle actin, and Nestin, after differentiation (Fig. 5A). In general, immunofluorescence staining did not reveal obvious defects in endodermal, mesodermal, or ectodermal differentiation of miPSCs with each Cisd2 genotype. Nevertheless, qRT-PCR indicated that several markers specific for the differentiation of the three dermal lineages were substantially decreased in Cisd2$^{-/-}$ miPSCs (*Ncam1*, *Olig2*, *Fgf5*, and *En2* as ectodermal markers; *Bmp4*, *T*, *Tbx3*, and *Bmp2* as mesodermal markers; and *Hnf4a*, *Gata6*, *Sox7*, and *Sox17* as endodermal

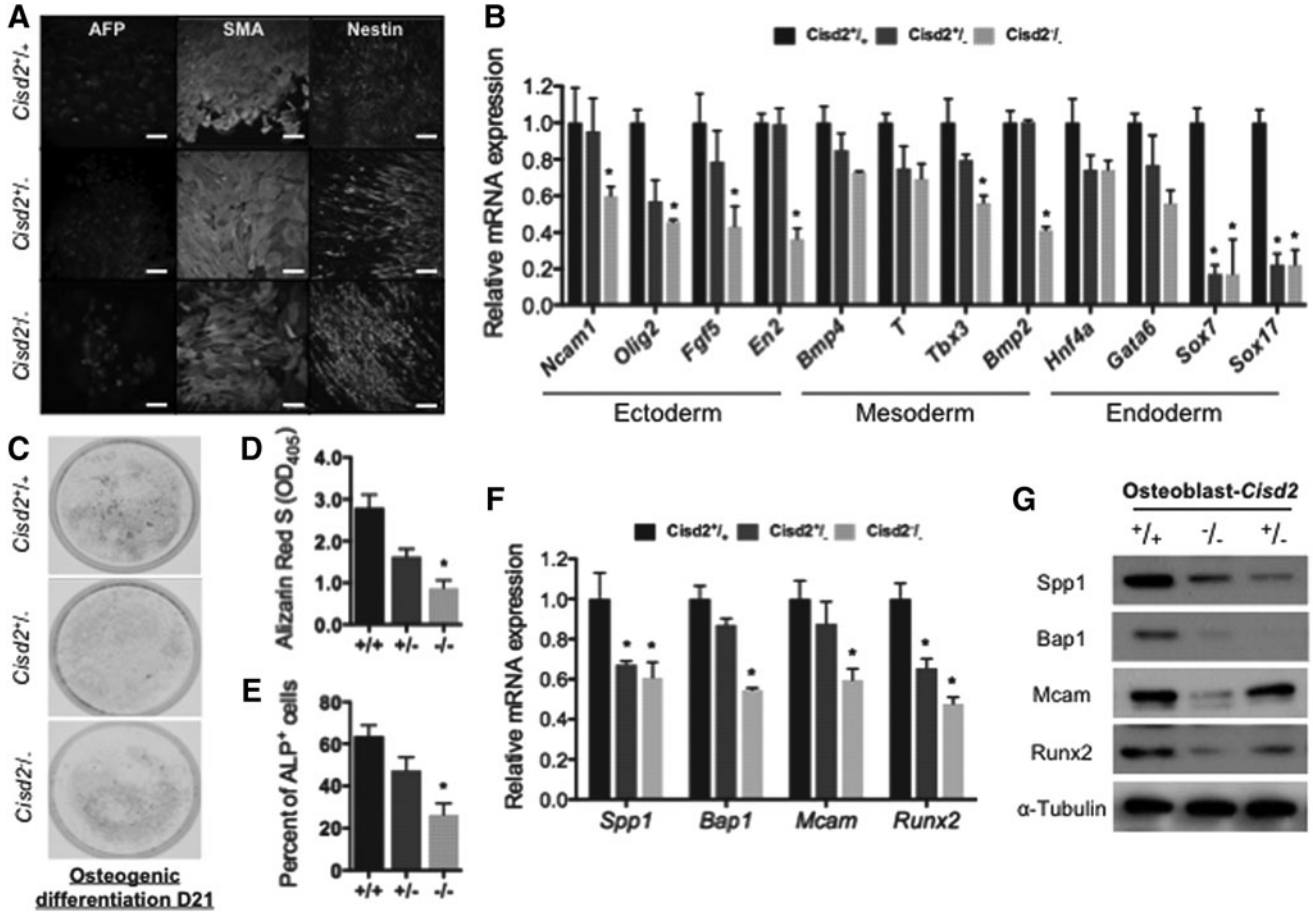

FIG. 5. Cisd2 deficiency impairs osteogenesis in miPSCs. **(A)** In vitro differentiation into all three germ layers. Immunofluoscence staining of miPSC lines derived cells of all three germ layers: endoderm (α-fetoprotein, AFP), mesoderm (smooth muscle actin, SMA), and ectoderm (Nestin). (Scale bar = 100 μm). **(B)** Quantitative RT-PCR analysis of developmental markers specifically for the differentiation of three dermal lineages. **(C)** Alizarin red S (ARS) staining of osteogenic differentiated miPSCs (21 days). **(D)** For quantitative analysis of the mineralization in osteoblast-like cells, ARS-stained red calcium deposits were dissolved in cetylpyridinium chloride buffer and quantified based on absorbance at 550 nm. **(E)** After allowing osteogenic differentiation for 14 days, flow cytometric analysis for surface ALP expression in osteocyte-differentiated miPSCs were analyzed *Cisd2*$^{+/+}$, *Cisd2*$^{+/-}$, and *Cisd2*$^{-/-}$ miPSCs. **(F)** After allowing osteogenic differentiation for 14 days, the expression levels of the Wnt downstream targets were analyzed in *Cisd2*$^{+/+}$, *Cisd2*$^{+/-}$, and *Cisd2*$^{-/-}$ miPSCs. **(G)** Western blot analysis of the osteo-progenitor proteins in the *Cisd2*$^{+/+}$, *Cisd2*$^{+/-}$, and *Cisd2*$^{-/-}$ miPSCs. α-Tubulin was used as a loading control. Data represent mean ± SD in independent experiment. $^{*}P < 0.05$.

markers; Fig. 5B). These data indicate that Cisd2 deficiency blunts the capacity of miPSCs for differentiation into multiple dermal lineages.

Recent studies have reported that the Wnt pathway is highly associated with osteogenesis in mouse embryonic stem cells [43]; therefore, we examined whether Cisd2 also influences the osteogenic potential of miPSCs. After employing the protocol for the generation of osteoblasts from miPSCs with various Cisd2 genotypes, ARS staining was used to examine Ca^{2+}-rich deposits in miPSCs that had differentiated into osteoblasts (Fig. 5C). A cetylpyridinium chloride solution was then used for extraction of ARS from cells and subsequent quantification of Ca^{2+}-rich deposits in these extracts via colorimetric detection at 405 nm [44]. Among all miPSCs with the various Cisd2 genotypes, *Cisd2*$^{-/-}$ miPSCs exhibited the least amount of Ca^{2+} deposits (Fig. 5D). In addition, flow cytometry analysis revealed that the level of ALP, a well-accepted osteogenic marker, was also substantially decreased in *Cisd2*$^{-/-}$ miPSCs (Fig. 5E and Supplementary Fig. S1B). Further, qRT-PCR indicated that the levels of osteogenic markers, such as *Spp1*, *Bap1*, *Mcam*, and runt-related transcription factor 2 (*Runx2*), were decreased in these cells (Fig. 5F). Western blot analysis confirmed the downregulation of these markers at the protein level (Fig. 5G). Collectively, our findings indicate that Cisd2 deficiency resulted in impaired differentiation of various dermal lineages, in which prominent abnormalities were observed in osteogenic differentiation.

Cisd2 and Gimap5 co-regulate Ca^{2+} homeostasis in both MEFs and miPSCs

A recent study has shown that Cisd2 deficiency inhibits adipogenesis by affecting intracellular Ca^{2+} levels. In addition, Cisd2 and endogenous Gimap5 have been demonstrated to interact with each other [19]. Notably, cells lacking both Cisd2 and Gimap5 exhibit additive increases in intracellular Ca^{2+}, suggesting that these proteins are essential for controlling

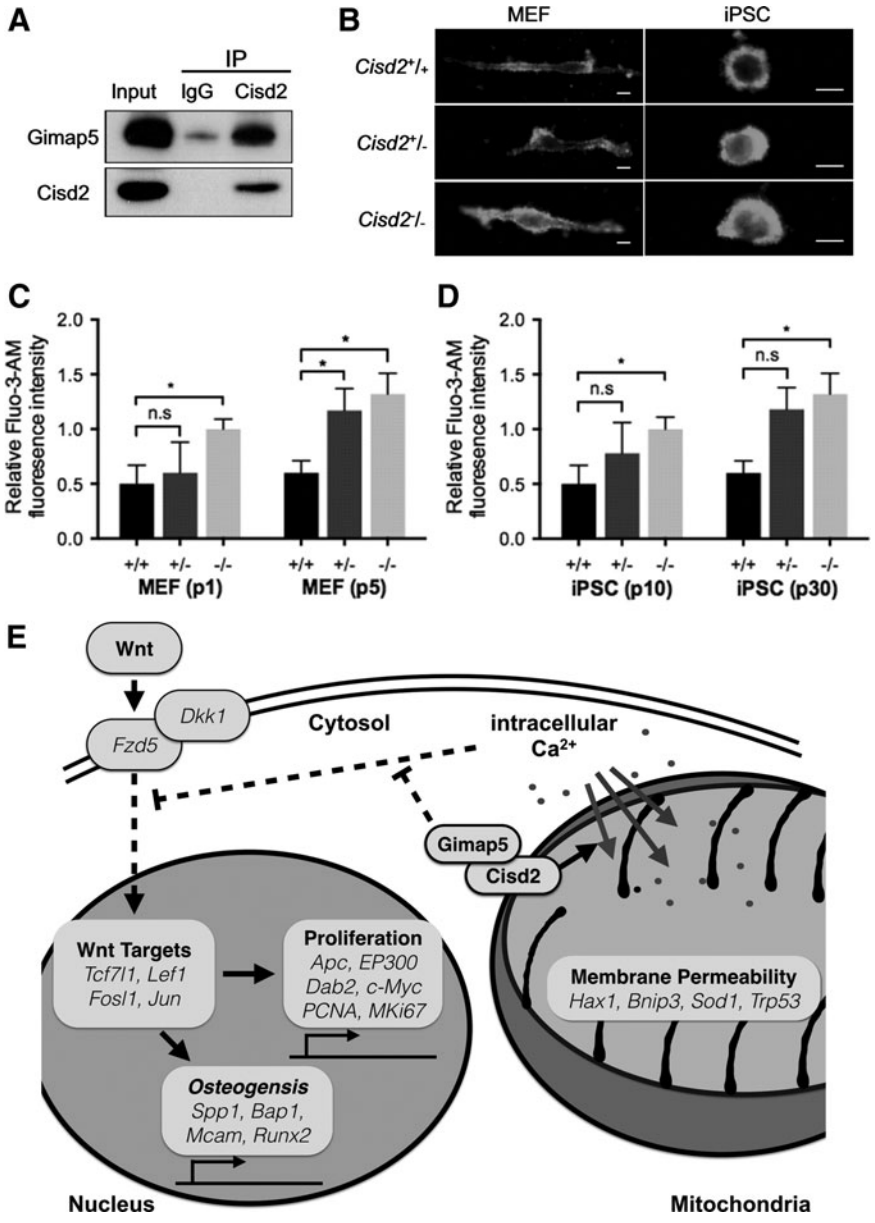

FIG. 6. Cisd2-mediated regulation of osteogenesis and Ca^{2+} homeostasis in miPSCs. **(A)** Co-immunoprecipitation assay of Cisd2 was performed in wild-type miPSCs. Immunoblot analysis using antibodies against Cisd2 and Gimap5 showed specific binding between Cisd2 and Gimap5. **(B)** Fluo-3-AM analysis reveals that Cisd2 deficiency induces high fluorescence intensity relative to Cisd2$^{+/+}$ in fibroblasts and miPSCs (Scale bar = 10 μm). **(C)** Relative Fluo-3/AM intensity in fibroblasts was measured by flow cytometry analysis. Compared to early passage, later passage Cisd2$^{-/-}$ fibroblasts and **(D)** Cisd2$^{-/-}$ miPSCs show increased intracellular Ca^{2+} levels. Data represent mean ± SD in independent experiment. $^*P < 0.05$. **(E)** Cisd2-mediated regulation of osteogenesis and Ca^{2+} homeostasis in miPSCs. Cisd2 deficiency increases the Ca^{2+} level in differentiating cells, which acts as a negative regulatory effect on Wnt/β-catenin signaling. This results in an inhibition on cell proliferation and osteogenesis.

intracellular Ca^{2+} levels [19]. To examine whether the interrelationship between Cisd2 and Gimap5 is also essential for regulation of Ca^{2+} homeostasis, several experiments were conducted to examine miPSCs with the genotype *Cisd2*$^{+/+}$, *Cisd2*$^{+/-}$, or *Cisd2*$^{-/-}$. The immunoprecipitation assay results showed that Cisd2 and Gimap5 interacted with each other in miPSCs (Fig. 6A). In addition, Cisd2$^{-/-}$ fibroblasts had higher intracellular Ca^{2+} levels in both MEFs and miPSCs compared with the corresponding cells with the other two Cisd2 genotypes, as determined using a Fluo-3-AM fluorescence probe (Fig. 6B). After continuous passaging, the intracellular Ca^{2+} levels remained the highest in Cisd$^{-/-}$ cells compared with *Cisd2*$^{+/+}$ and *Cisd2*$^{+/-}$ cells (Fig. 6C, D), and these high Ca^{2+} levels under Cisd2 deficiency were observed in both MEFs (Fig. 6C) and miPSCs (Fig. 6D). These results suggest that the association of Cisd2 with Gimap5 contributes to the maintenance of intracellular Ca^{2+} homeostasis in both somatic and stem cells and that Cisd2 deficiency contributes to abnormal elevations in intracellular Ca^{2+} concentrations and impaired mitochondrial function, which may negatively affect regular Wnt pathway signaling (Fig. 6E).

Discussion

Cisd2 is a member of the CDGSH iron-sulfur cluster family, which maintains mitochondrial integrity and regulates the life span and development of multiple cell lineages [30]. A mutation in *Cisd2* is a major cause of Wolfram syndrome, an autosomal recessive inherited disease that is characterized by multiple degenerative anomalies [7]. *Cisd2* KO mice exhibit significant clinical features, including neurodegeneration of the central and peripheral nervous systems, decreased muscle mass, osteopenia, and lordokyphosis [7]. In addition, Cisd2 deficiency inhibits adipocyte differentiation in mice [19]. These findings indicate a critical but unclear role of Cisd2 during development. Cisd2 forms a homodimer that harbors two redox-active 2Fe-2S clusters and localizes to the ER or mitochondrial membrane [7,31]. Mitochondrial functions may play critical roles in controlling the early differentiation of embryonic stem cells [16]. To understand the importance of Cisd2 in development, we established miPSCs from *Cisd2*$^{-/-}$ mice for the first time to investigate the progression of reprogramming, pluripotency maintenance, and differentiation. Cisd2 deficiency induced mitochondrial dysfunction, which was associated with reductions in membrane potential, mitochondrial mass, and expression of genes encoding electron transport chain proteins. Interestingly, we observed that Cisd2 deficiency enhanced the efficacy of reprograming but decreased the growth rate and efficiency of osteogenesis. Microarray analysis revealed that the major influence on osteogenic differentiation was the commitment of *Cisd2*$^{-/-}$ miPSCs toward an osteoclast fate. Collectively, our data suggest that Cisd2-dependent mitochondrial integrity may be fundamental for maintaining the growth rate of miPSCs and the differentiation efficacy of osteogenesis.

Cisd2 is involved in mitochondrial membrane potential maintenance

Classification of mitochondrial proteins into several groups according to their specific functions revealed that the expression levels of the proteins associated with membrane potential were severely decreased in *Cisd2*$^{-/-}$ miPSCs. This finding is remarkable because *Cisd2* KO mice have been previously shown to exhibit obvious impairments in the functioning of mitochondrial complexes I and III [7], whereas our bioinformatics analysis indicated that mitochondrial membrane potential-associated proteins were primarily destroyed, particularly during the embryonic stages [7]. The mitochondrial membrane potential controls the release of cytochrome c to mediate cellular apoptosis [45]. Reducing the membrane potential has been shown to stimulate G0/G1 arrest to diminish cell growth without inducing apoptosis in colonic epithelial cells and promyelocytic leukemia cells [46,47]. These findings are consistent with our results, indicating that Cisd2 regulates the membrane potential, thereby promoting cellular growth.

Cisd2 determines mesodermal differentiation

Mitochondria-enriched organs, such as those of the nervous system, exhibit significant abnormalities in *Cisd2* KO mice [7]. Most of these organs develop from the ectodermal lineage, and the mesoderm is not considered the primary impaired germ layer. Lordokyphosis and osteoporosis have been previously noted as significant phenotypes in *Cisd2* KO mice after 8 weeks of age, emphasizing the importance of Cisd2 in mesodermal development [7]. The easily manipulable miPSC platform provided insights into the influence of Cisd2 during the embryonic stage. *Cisd2*$^{-/-}$ miPSCs exhibited lower expression levels of several mesodermal markers compared with wild-type miPSCs, as determined by qRT-PCR. Interestingly, some of these mesodermal markers are also endodermal markers, such as *Sox7* and *Sox17*, which were significantly downregulated [48]. Sox17 deficiency suppresses the mesodermal transcription factors Mesp1 and Mesp2, inhibiting cardiomyocyte genesis. Sox7 functions in Flk1 mesodermal precursors, and Sox7 shRNA prevents formation of hematopoietic progenitors [48–51]. Two other notable mesodermal markers are Bmp2 and Bmp4. The Bmp family regulates critical determining factors involved in formation of the mesoderm, heart, cartilage, and bone. Bmp2 stimulates the expression of bone-associated markers, such as osteocalcin, by activating downstream Smad 1/5 cross-linked to Runx2. Bmp4 is a crucial factor for transmitting signals from the extracellular matrix (ECM) to intracellular signaling pathways [52–54]. Heteromeric complexes formed by β3-integrin and Bmp4 receptor BMPRIA upon Bmp4 stimulation promote the activity of Erk2 and Smad1/5 to arrest the cell cycle at G0/G1 via upregulation of p21 and p27, which initiates differentiation, particularly osteogenesis [55,56]. The significant inhibition of expression of the early to late mesodermal markers Sox7/Sox17 and Bmp2/Bmp4 in *Cisd2*$^{-/-}$ miPSCs indicates that Cisd2 has an essential role in cell fate determination.

Cisd2 is involved in osteogenic differentiation

Consistent with the analytical results, ARS staining revealed osteogenic variations between *Cisd2*$^{+/+}$ and *Cisd2*$^{-/-}$ miPSCs. RNA expression analysis indicated that the expression levels of most of the precursor and mature markers of osteoblasts, such as *Spp1*, *Bap1*, *Mcam*, and *Runx2*, were reduced, further emphasizing the importance of Cisd2 in osteogenesis. *Runx2* is a key transcription factor that serves

as a scaffold for nucleic acids and regulates several essential skeletal-related genes [57]. It acts bidirectionally to target the promoter of Bmp2/Bmp4 and recruit R-Smad to trigger Bmp signaling pathways [43,58–61]. Interestingly, nearly all of the genes with the most drastically altered expression function downstream of the Wnt pathway, indicating that Cisd2 is involved in this signaling pathway through an unknown mechanism during the osteogenic process.

Wnt and Bmp4 are two well-known signals involved in osteophysiology [43,58,59]. Canonical Wnt signaling is initiated when Wnt3a binds to Lrp5/6 and Fzd, consequently dephosphorylating β-catenin and enabling its interaction with Tcf/Lef to promote the activation of downstream targets, including Runx2, Fosl, and Jun [58,62]. Wnt is involved in many pivotal cellular physiological processes, including proliferation, differentiation, and the ECM mineralization of osteoblasts [62,63]. It also blocks the conversion of mesenchymal cells into adipocytes [64] and the differentiation of chondrocytes [65]. Bmp2 is induced downstream to promote Runx2 expression, which is upregulated during osteogenesis. The Wnt pathway reportedly interacts with Bmp signaling and vice versa. For example, Bmp2 inhibits Wnt7a and β-catenin via p38 to enhance chondrogenesis, whereas their co-regulation reduces osteoblast differentiation [66]. However, studies of the involvement of Cisd2 in the crosstalk between these two signaling pathways to direct osteogenesis are limited. Overexpression of mitochondrial transcription factor A (Tfam) activates the canonical Wnt pathway through Lrp5 to promote β-catenin/Tcf transcriptional activity, further contributing to the induction of osteogenesis-related gene expression [67]. Bmp2 also functions as an apoptotic regulator of osteoblasts by inducing the mitochondrial release of cytochrome c and Bax/Bcl-2 [68,69]. Collectively, these recent studies have demonstrated the importance of the mitochondrion in the Wnt/Bmp signaling pathway, but the detailed mechanism remains to be further elucidated. Bone remodeling is a balanced state between bone formation and bone resorption involving interactions between osteoblasts and osteoclasts [70]. Clinical findings have indicated that imbalances between bone formation and resorption lead to mineral overaccumulation and the subsequent stimulation of abnormal growth, resulting in lordokyphosis and osteoporosis [70,71]. As previously mentioned, the Wnt/β-catenin and Bmp pathways are the two most critical signaling pathways that mediate bone formation [72]. Bmps act synergistically with Wnt to inactivate GSK3β, thereby stabilizing β-catenin, which upregulates *Runx2* expression [72]. The Wnt and Bmp pathways collaborate in several biogenic processes, particularly during the early stages of differentiation [73]. In addition to the molecular mechanism driving osteodifferentiation, bone remodeling is regarded as a reversible process. Osteoblasts are the major regulators of osteoclastogenesis through the binding of the surface marker M-CSF to c-FMS, activating NF-κB/c-Fos to induce the expression of osteoclast-associated proteins or the secretion of osteoprotegerin, which interferes with the RANKL pathway in osteoclast progenitors [74,75]. Osteoblasts and osteoclasts vary slightly in structure. Osteoblasts have an abundance of ERs, whereas osteoclasts are enriched in mitochondria [76]. Because Cisd2 is important in the mitochondria, we speculate that osteoclastogenesis is likely disrupted, consistent with our findings, but the underlying mechanism is unclear. Cisd2 was defined as the pivotal gene in WFS2 due to its role in the ER, acting together with Bcl-2, to modulate Ca^{2+} homeostasis [4,5]. This role has also been described by Wang et al., who demonstrated that Cisd2 is localized to mitochondria-associated ER membranes [19], indicating that this protein maintains not only the function of mitochondria but also that of the ER [77]. Therefore, osteoporosis induced by the loss of Cisd2 function may be caused by abnormal Ca^{2+} deposition in the ER.

Dkk1 specifically inhibits canonical Wnt signaling by binding to the Wnt-receptor complex [41]. In addition, transmembrane protein Kremen2 are high-affinity Dkk1 receptors that functionally cooperate with Dkk1 to block Wnt/beta-catenin signaling. Kremen2 forms a ternary complex with Dkk1 and Lrp6, and induces rapid endocytosis and removal of the Wnt-receptor complex from the plasma membrane. Our results indicated that $Cisd2^{-/-}$ iPSCs contained higher amount of phosphorylated β-catenin than the other two Cisd2 counterpart lines. Remarkably, Cisd2 deficiency substantially upregulated Dkk1 but did not affect Kremen2 protein amount (Fig. 3F). These data indicated that regulation of Wnt pathway by Cisd2, at least, is partially exerted through modulating Dkk1 to antagonizing the signaling of Wnt pathway.

Taken together, these findings suggest that the expression of Cisd2 and the Cisd2-related pathway may affect osteogenic differentiation and that osteogenesis-related signaling candidates may respond to the activities of Cisd2. Future studies should determine whether the two above-mentioned signaling pathways participate in crosstalk through Cisd2 to regulate dynamic bone remodeling and should further clarify the role of Cisd2 in relation to the mitochondrion and ER in osteophysiology (Fig. 6E).

Our study reports the promising generation of miPSCs from *Cisd2* KO mice that recapitulate developmental and differentiation processes. We have demonstrated that the loss of Cisd2 decreases the efficiency of osteogenic differentiation and affects certain aspects of mitochondrial function via undetermined mechanisms in Cisd2-deficient miPSCs. Notably, the role of Cisd2 in the differentiation and development of specific lineages, particularly those related to the aging process and senescence, should be further explored. Moreover, through the application of cellular reprogramming and ex vivo transplantation, we hope to better understand the Cisd2-associated biomolecular mechanisms and Cisd2-dependent premature aging process, and this information will potentially be of benefit to researchers of related clinical syndromes, such as WFS2.

Acknowledgments

This study was funded by the Ministry of Health and Welfare [Excellent Clinical Trial Center & Cancer Center Research of Excellence (MOHW104-TDU-B-211-124-001/TD-B-111-02 & MOHW104-TDU-B-211-113-003)], National Health Research Institutes (NHRI-EX102-10258SI), MOST (103-2321-B-010-025, 104-2627-M-010-004,104-2325-B-010-006), MOST Ingenious Plan (NYMU-NHRI-2015), Yen-Tjing-Ling Medical Foundation (CI-102/103/104), TVGH-NTU Joint Project (VN104-09), Taipei Veterans General Hospital (103-V-B-027), National Health Research Institutes (NHRI-EX104-10258SI), and the Genomic Center Project and Cancer Center

Project of National Yang-Ming University (Ministry of Education, Aim for the Top University Plan), Taiwan.

Author Disclosure Statement

No competing financial interests exist.

References

1. Wiley SE, AY Andreyev, AS Divakaruni, R Karisch, G Perkins, EA Wall, P van der Geer, YF Chen, TF Tsai, et al. (2013). Wolfram Syndrome protein, Miner1, regulates sulphydryl redox status, the unfolded protein response, and Ca2+ homeostasis. EMBO Mol Med 5:904–918.
2. Wiley SE, AN Murphy, SA Ross, P van der Geer and JE Dixon. (2007). MitoNEET is an iron-containing outer mitochondrial membrane protein that regulates oxidative capacity. Proc Natl Acad Sci U S A 104:5318–5323.
3. Taminelli GL, V Sotomayor, AG Valdivieso, ML Teiber, MC Marin and TA Santa-Coloma. (2008). CISD1 codifies a mitochondrial protein upregulated by the CFTR channel. Biochem Biophys Res Commun 365:856–862.
4. Chang NC, M Nguyen, M Germain and GC Shore. (2010). Antagonism of Beclin 1-dependent autophagy by BCL-2 at the endoplasmic reticulum requires NAF-1. EMBO J 29:606–618.
5. Chang NC, M Nguyen, J Bourdon, PA Risse, J Martin, G Danialou, R Rizzuto, BJ Petrof and GC Shore. (2012). Bcl-2-associated autophagy regulator Naf-1 required for maintenance of skeletal muscle. Hum Mol Genet 21:2277–2287.
6. Kanki T and DJ Klionsky. (2009). Mitochondrial abnormalities drive cell death in Wolfram syndrome 2. Cell Res 19:922–923.
7. Chen YF, CH Kao, YT Chen, CH Wang, CY Wu, CY Tsai, FC Liu, CW Yang, YH Wei, et al. (2009). Cisd2 deficiency drives premature aging and causes mitochondria-mediated defects in mice. Genes Dev 23:1183–1194.
8. Chen CT, SH Hsu and YH Wei. (2012). Mitochondrial bioenergetic function and metabolic plasticity in stem cell differentiation and cellular reprogramming. Biochim Biophys Acta 1820:571–576.
9. DiMauro S and EA Schon. (2003). Mitochondrial respiratory-chain diseases. N Engl J Med 348:2656–2668.
10. Bukowiecki R, J Adjaye and A Prigione. (2014). Mitochondrial function in pluripotent stem cells and cellular reprogramming. Gerontology 60:174–182.
11. Ruiz S, AD Panopoulos, A Herrerias, KD Bissig, M Lutz, WT Berggren, IM Verma and JC Izpisua Belmonte. (2011). A high proliferation rate is required for cell reprogramming and maintenance of human embryonic stem cell identity. Curr Biol 21:45–52.
12. Wallace DC. (1999). Mitochondrial diseases in man and mouse. Science 283:1482–1488.
13. Moyes CD, OA Mathieu-Costello, N Tsuchiya, C Filburn and RG Hansford. (1997). Mitochondrial biogenesis during cellular differentiation. Am J Physiol 272:C1345–C1351.
14. Atmani H, D Chappard and MF Basle. (2003). Proliferation and differentiation of osteoblasts and adipocytes in rat bone marrow stromal cell cultures: effects of dexamethasone and calcitriol. J Cell Biochem 89:364–372.
15. Lonergan T, C Brenner and B Bavister. (2006). Differentiation-related changes in mitochondrial properties as indicators of stem cell competence. J Cell Physiol 208:149–153.
16. Mandal S, AG Lindgren, AS Srivastava, AT Clark and U Banerjee. (2011). Mitochondrial function controls proliferation and early differentiation potential of embryonic stem cells. Stem Cells 29:486–495.
17. Facucho-Oliveira JM, J Alderson, EC Spikings, S Egginton and JC St John. (2007). Mitochondrial DNA replication during differentiation of murine embryonic stem cells. J Cell Sci 120:4025–4034.
18. Chen CT, YR Shih, TK Kuo, OK Lee and YH Wei. (2008). Coordinated changes of mitochondrial biogenesis and antioxidant enzymes during osteogenic differentiation of human mesenchymal stem cells. Stem Cells 26:960–968.
19. Wang CH, YF Chen, CY Wu, PC Wu, YL Huang, CH Kao, CH Lin, LS Kao, TF Tsai and YH Wei. (2014). Cisd2 modulates the differentiation and functioning of adipocytes by regulating intracellular Ca2+ homeostasis. Hum Mol Genet 23:4770–4785.
20. Takahashi K, K Tanabe, M Ohnuki, M Narita, T Ichisaka, K Tomoda and S Yamanaka. (2007). Induction of pluripotent stem cells from adult human fibroblasts by defined factors. Cell 131:861–872.
21. Takahashi K and S Yamanaka. (2006). Induction of pluripotent stem cells from mouse embryonic and adult fibroblast cultures by defined factors. Cell 126:663–676.
22. Chiou SH, BH Jiang, YL Yu, SJ Chou, PH Tsai, WC Chang, LK Chen, LH Chen, Y Chien and GY Chiou. (2013). Poly(ADP-ribose) polymerase 1 regulates nuclear reprogramming and promotes iPSC generation without c-Myc. J Exp Med 210:85–98.
23. Sung LY, S Gao, H Shen, H Yu, Y Song, SL Smith, CC Chang, K Inoue, L Kuo, et al. (2006). Differentiated cells are more efficient than adult stem cells for cloning by somatic cell nuclear transfer. Nat Genet 38:1323–1328.
24. Cossarizza A, M Baccarani-Contri, G Kalashnikova and C Franceschi. (1993). A new method for the cytofluorimetric analysis of mitochondrial membrane potential using the J-aggregate forming lipophilic cation 5,5′,6,6′-tetrachloro-1,1′,3,3′-tetraethylbenzimidazolcarbocyanine iodide (JC-1). Biochem Biophys Res Commun 197:40–45.
25. Smiley ST, M Reers, C Mottola-Hartshorn, M Lin, A Chen, TW Smith, GD Steele, Jr. and LB Chen. (1991). Intracellular heterogeneity in mitochondrial membrane potentials revealed by a J-aggregate-forming lipophilic cation JC-1. Proc Natl Acad Sci U S A 88:3671–3675.
26. Mancini M, M Sedghinasab, K Knowlton, A Tam, D Hockenbery and BO Anderson. (1998). Flow cytometric measurement of mitochondrial mass and function: a novel method for assessing chemoresistance. Ann Surg Oncol 5:287–295.
27. Koch P, T Opitz, JA Steinbeck, J Ladewig and O Brustle. (2009). A rosette-type, self-renewing human ES cell-derived neural stem cell with potential for in vitro instruction and synaptic integration. Proc Natl Acad Sci U S A 106:3225–3230.
28. Weidgang CE, R Russell, PR Tata, SJ Kuhl, A Illing, M Muller, Q Lin, C Brunner, TM Boeckers, et al. (2013). TBX3 directs cell-fate decision toward mesendoderm. Stem Cell Reports 1:248–265.
29. Finger JH, CM Smith, TF Hayamizu, IJ McCright, JT Eppig, JA Kadin, JE Richardson and M Ringwald. (2011). The mouse gene expression database (GXD): 2011 update. Nucleic Acids Res 39:D835–D841.
30. Chen YF, CH Kao, R Kirby and TF Tsai. (2009). Cisd2 mediates mitochondrial integrity and life span in mammals. Autophagy 5:1043–1045.

31. Conlan AR, HL Axelrod, AE Cohen, EC Abresch, J Zuris, D Yee, R Nechushtai, PA Jennings and ML Paddock. (2009). Crystal structure of Miner1: The redox-active 2Fe-2S protein causative in Wolfram Syndrome 2. J Mol Biol 392:143–153.
32. Van Gansen P and N Van Lerberghe. (1988). Potential and limitations of cultivated fibroblasts in the study of senescence in animals. A review on the murine skin fibroblasts system. Arch Gerontol Geriatr 7:31–74.
33. Vafiadaki E, DA Arvanitis, SN Pagakis, V Papalouka, D Sanoudou, A Kontrogianni-Konstantopoulos and EG Kranias. (2009). The anti-apoptotic protein HAX-1 interacts with SERCA2 and regulates its protein levels to promote cell survival. Mol Biol Cell 20:306–318.
34. Vande Velde C, J Cizeau, D Dubik, J Alimonti, T Brown, S Israels, R Hakem and AH Greenberg. (2000). BNIP3 and genetic control of necrosis-like cell death through the mitochondrial permeability transition pore. Mol Cell Biol 20: 5454–5468.
35. Aquilano K, P Vigilanza, G Rotilio and MR Ciriolo. (2006). Mitochondrial damage due to SOD1 deficiency in SH-SY5Y neuroblastoma cells: a rationale for the redundancy of SOD1. FASEB J 20:1683–1685.
36. Vaseva AV and UM Moll. (2009). The mitochondrial p53 pathway. Biochim Biophys Acta 1787:414–420.
37. Martin BL and D Kimelman. (2008). Regulation of canonical Wnt signaling by Brachyury is essential for posterior mesoderm formation. Dev Cell 15:121–133.
38. Lindsley RC, JG Gill, M Kyba, TL Murphy and KM Murphy. (2006). Canonical Wnt signaling is required for development of embryonic stem cell-derived mesoderm. Development 133:3787–3796.
39. MacDonald BT, K Tamai and X He. (2009). Wnt/beta-catenin signaling: components, mechanisms, and diseases. Dev Cell 17:9–26.
40. Matsuo K, JM Owens, M Tonko, C Elliott, TJ Chambers and EF Wagner. (2000). Fosl1 is a transcriptional target of c-Fos during osteoclast differentiation. Nat Genet 24:184–187.
41. Niida A, T Hiroko, M Kasai, Y Furukawa, Y Nakamura, Y Suzuki, S Sugano and T Akiyama. (2004). DKK1, a negative regulator of Wnt signaling, is a target of the beta-catenin/TCF pathway. Oncogene 23:8520–8526.
42. van Es JH, N Barker and H Clevers. (2003). You Wnt some, you lose some: oncogenes in the Wnt signaling pathway. Curr Opin Genet Dev 13:28–33.
43. Gaur T, CJ Lengner, H Hovhannisyan, RA Bhat, PV Bodine, BS Komm, A Javed, AJ van Wijnen, JL Stein, GS Stein and JB Lian. (2005). Canonical WNT signaling promotes osteogenesis by directly stimulating Runx2 gene expression. J Biol Chem 280:33132–33140.
44. Gregory CA, WG Gunn, A Peister and DJ Prockop. (2004). An Alizarin red-based assay of mineralization by adherent cells in culture: comparison with cetylpyridinium chloride extraction. Anal Biochem 329:77–84.
45. Vladimirov YA, EV Proskurnina and AV Alekseev. (2013). Molecular mechanisms of apoptosis. structure of cytochrome c-cardiolipin complex. Biochemistry 78:1086–1097.
46. Mandal S, P Guptan, E Owusu-Ansah and U Banerjee. (2005). Mitochondrial regulation of cell cycle progression during development as revealed by the tenured mutation in Drosophila. Dev Cell 9:843–854.
47. Owusu-Ansah E, A Yavari, S Mandal and U Banerjee. (2008). Distinct mitochondrial retrograde signals control the G1-S cell cycle checkpoint. Nat Genet 40:356–361.
48. Niimi T, Y Hayashi, S Futaki and K Sekiguchi. (2004). SOX7 and SOX17 regulate the parietal endoderm-specific enhancer activity of mouse laminin alpha1 gene. J Biol Chem 279:38055–38061.
49. Bondue A, G Lapouge, C Paulissen, C Semeraro, M Iacovino, M Kyba and C Blanpain. (2008). Mesp1 acts as a master regulator of multipotent cardiovascular progenitor specification. Cell Stem Cell 3:69–84.
50. Nelson TJ, A Chiriac, RS Faustino, RJ Crespo-Diaz, A Behfar and A Terzic. (2009). Lineage specification of Flk-1+progenitors is associated with divergent Sox7 expression in cardiopoiesis. Differentiation 77:248–255.
51. Gandillet A, AG Serrano, S Pearson, ALM Lie, G Lacaud and V Kouskoff. (2009). Sox7-sustained expression alters the balance between proliferation and differentiation of hematopoietic progenitors at the onset of blood specification. Blood 114:4813–4822.
52. Mukherjee A and P Rotwein. (2009). Akt promotes BMP2-mediated osteoblast differentiation and bone development. J Cell Sci 122:716–726.
53. Phimphilai M, Z Zhao, H Boules, H Roca and RT Franceschi. (2006). BMP signaling is required for RUNX2-dependent induction of the osteoblast phenotype. J Bone Miner Res 21:637–646.
54. Wang YK, X Yu, DM Cohen, MA Wozniak, MT Yang, L Gao, J Eyckmans and CS Chen. (2012). Bone morphogenetic protein-2-induced signaling and osteogenesis is regulated by cell shape, RhoA/ROCK, and cytoskeletal tension. Stem Cells Dev 21:1176–1186.
55. Marie PJ, E Hay and Z Saidak. (2014). Integrin and cadherin signaling in bone: role and potential therapeutic targets. Trends Endocrinol Metab 25:567–575.
56. Chang SF, TK Chang, HH Peng, YT Yeh, DY Lee, CR Yeh, J Zhou, CK Cheng, CA Chang and JJ Chiu. (2009). BMP-4 induction of arrest and differentiation of osteoblast-like cells via p21 CIP1 and p27 KIP1 regulation. Mol Endocrinol 23:1827–1838.
57. Jonason JH, G Xiao, M Zhang, L Xing and D Chen. (2009). Post-translational regulation of Runx2 in bone and cartilage. J Dent Res 88:693–703.
58. Marcellini S, JP Henriquez and A Bertin. (2012). Control of osteogenesis by the canonical Wnt and BMP pathways in vivo: cooperation and antagonism between the canonical Wnt and BMP pathways as cells differentiate from osteochondroprogenitors to osteoblasts and osteocytes. Bioessays 34:953–962.
59. Yaccoby S. (2010). The role of the proteasome in bone formation and osteoclastogenesis. IBMS BoneKEy 7:147–155.
60. Zhang X, J Akech, G Browne, S Russell, JJ Wixted, JL Stein, GS Stein and JB Lian. (2015). Runx2-smad signaling impacts the progression of tumor-induced bone disease. Int J Cancer 136:1321–1332.
61. Javed A, JS Bae, F Afzal, S Gutierrez, J Pratap, SK Zaidi, Y Lou, AJ van Wijnen, JL Stein, GS Stein and JB Lian. (2008). Structural coupling of Smad and Runx2 for execution of the BMP2 osteogenic signal. J Biol Chem 283: 8412–8422.
62. Brunt KR, Y Zhang, A Mihic, M Li, S-H Li, P Xue, W Zhang, S Basmaji, K Tsang, et al. (2012). Role of WNT/β-catenin signaling in rejuvenating myogenic differentiation of aged mesenchymal stem cells from cardiac patients. Am J Pathol 181:2067–2078.
63. Kim JH, X Liu, J Wang, X Chen, H Zhang, SH Kim, J Cui, R Li, W Zhang, et al. (2013). Wnt signaling in bone for-

mation and its therapeutic potential for bone diseases. Ther Adv Musculoskelet Dis 5:13–31.
64. Longo KA, WS Wright, S Kang, I Gerin, SH Chiang, PC Lucas, MR Opp and OA MacDougald. (2004). Wnt10b inhibits development of white and brown adipose tissues. J Biol Chem 279:35503–35509.
65. Hwang SG, SS Yu, SW Lee and JS Chun. (2005). Wnt-3a regulates chondrocyte differentiation via c-Jun/AP-1 pathway. FEBS Lett 579:4837–4842.
66. Jin EJ, SY Lee, YA Choi, JC Jung, OS Bang and SS Kang. (2006). BMP-2-enhanced chondrogenesis involves p38 MAPK-mediated down-regulation of Wnt-7a pathway. Mol Cells 22:353–359.
67. Yoon JC, A Ng, BH Kim, A Bianco, RJ Xavier and SJ Elledge. (2010). Wnt signaling regulates mitochondrial physiology and insulin sensitivity. Genes Dev 24:1507–1518.
68. Sugimori K, K Matsui, H Motomura, T Tokoro, J Wang, S Higa, T Kimura and I Kitajima. (2005). BMP-2 prevents apoptosis of the N1511 chondrocytic cell line through PI3K/Akt-mediated NF-kappaB activation. J Bone Miner Metab 23:411–419.
69. Hyzy SL, R Olivares-Navarrete, Z Schwartz and BD Boyan. (2012). BMP2 induces osteoblast apoptosis in a maturation state and noggin-dependent manner. J Cell Biochem 113: 3236–3245.
70. Raisz LG. (1999). Physiology and pathophysiology of bone remodeling. Clin Chem 45:1353–1358.
71. Ti YF, R Wang and JN Zhao. (2014). [Mechanism of osteoclast in bone resorption]. Zhongguo Gu Shang 27: 529–532.
72. Baker JC, RS Beddington and RM Harland. (1999). Wnt signaling in Xenopus embryos inhibits bmp4 expression and activates neural development. Genes Dev 13:3149–3159.
73. Kamiya N, T Kobayashi, Y Mochida, PB Yu, M Yamauchi, HM Kronenberg and Y Mishina. (2010). Wnt inhibitors Dkk1 and Sost are downstream targets of BMP signaling through the type IA receptor (BMPRIA) in osteoblasts. J Bone Miner Res 25:200–210.
74. Glantschnig H, JE Fisher, G Wesolowski, GA Rodan and AA Reszka. (2003). M-CSF, TNFalpha and RANK ligand promote osteoclast survival by signaling through mTOR/S6 kinase. Cell Death Differ 10:1165–1177.
75. Faccio R, S Takeshita, A Zallone, FP Ross and SL Teitelbaum. (2003). c-Fms and the alphavbeta3 integrin collaborate during osteoclast differentiation. J Clin Invest 111:749–758.
76. Capulli M, R Paone and N Rucci. (2014). Osteoblast and osteocyte: games without frontiers. Arch Biochem Biophys 561:3–12.
77. Chang NC, M Nguyen and GC Shore. (2012). BCL2-CISD2: An ER complex at the nexus of autophagy and calcium homeostasis? Autophagy 8:856–857.

Address correspondence to:
Dr. Yi-Yen Lee
Department of Neurosurgery
Neurological Institute
Taipei Veterans General Hospital
No. 201, Sec. 2, Shih-Pai Road
Taipei 11217
Taiwan

E-mail: yylee62@gmail.com

Dr. Shih-Hwa Chiou
Department of Medical Research
Taipei Veterans General Hospital
No. 201, Sec. 2, Shih-Pai Road
Taipei 11217
Taiwan

E-mail: shchiou@vghtpe.gov.tw

Received for publication February 17, 2015
Accepted after revision July 7, 2015
Prepublished on Liebert Instant Online July 31, 2015